Dynamics of the South American Coastal Desert

MAGDA LUZIMAR DE ABREU

Centro de Previsão de Tempo e Estudos Climáticos—CPTEC, Instituto Nacional de Pesquisas Espaciais, São Paulo, Brazil

PETER R. BANNON

Department of Meteorology, The Pennsylvania State University, University Park, Pennsylvania

(Manuscript received 22 June 1992, in final form 27 January 1993)

ABSTRACT

The world's driest coastal desert is in South America along the coasts of Peru and Chile. The desert's maintenance is investigated by studying the local dynamics of the low-level southerly flow along the coast. A linear boundary-layer model is used in which a Boussinesq atmosphere is driven by a surface thermal contrast on a β plane. The resting basic state is stably stratified. Constant mechanical and thermal diffusivities are assumed in the momentum and heat equations, respectively. The dynamics of the buoyancy field is governed by a three-dimensional eighth-order differential equation in which the meridional dependence enters parametrically. Results are shown for different values of the constants involved as well as for solutions on an f plane and a semigeostrophic β plane.

The results indicate that the effect of nonuniform rotation is responsible for the presence of subsidence along the coast and inland. This coastal subsidence helps maintain the desert by increasing the static stability and suppressing deep convection. The predicted vertical wind profiles agree well with the observations for Lima, Peru. Sensitivity tests indicate that the flow depends on the interplay between stratification, friction, and the Coriolis parameter and its variation (β). The mechanical frictional effects are mainly constrained to a shallow Ekman layer, whereas the thermal effects are manifested in deeper layers controlled by the β effect.

1. Introduction

The world's driest coastal desert lies along the west coast of South America, extending from 8° to 30°S. It is the longest and driest coastal desert (Lydolph 1973) in the world. Iquique, Chile, has reportedly gone as long as ten years without measurable precipitation (Lettau 1978). The scarcity of water has motivated the harvesting of the stratocumulus cloud deck where this climatological feature meets the coastal mountains (Schemenauer et al. 1988).

Consistent with the lack of precipitation, the thermal structure of the coastal region is characterized by a strong low-level inversion (Prohaska 1973). This inversion lies near the 1-km level and has a strength of 10–15 K. It is a persistent climatological feature of the region. Typically, the inversion is lowest at the coast and increases in height offshore. The horizontal temperature contrast between the cold coastal waters and the warm land is about 5 K. Trewartha (1981) provides a good review of the climate of the region.

Climatological wind data (Oort 1983) indicate that the low-level flow along the desert is equatorward. Figure 1 shows the wind profile for Lima, Peru (12°S). Steady southerly winds (4 m s^{-1}) at the surface decrease with height and reverse direction aloft. In contrast to these southerlies, which are predominantly alongshore, there are weaker onshore winds (1 m s^{-1}), which become offshore above 300 m. The alongshore flow is stronger and deeper than the onshore flow.

Lettau (1978) modeled the wind profile using a theory of the Ekman layer with a thermal wind (Mahrt and Schwerdtfeger 1970); however the wind speeds predicted by this f-plane theory (10–20 m s^{-1}) were too strong. Later Enfield (1981) employed the same model with different parameter settings to obtain a reasonable fit to the observations for Lima. The model is limited by the need to prescribe the vertical structure of the horizontal temperature gradient.

The importance of the meridional variation of the Coriolis parameter has been emphasized by Riehl (1979) for the subtropical trade winds and by Smagorinsky (1953) for large-scale stationary waves in midlatitudes forced by zonally asymmetric heating. Smagorinsky considers a linear quasigeostrophic fluid with a basic-state westward zonal wind and an Ekman pumping formulation of boundary-layer process. Such a model fails to resolve the structure of the boundary layer and is inappropriate for the subtropical regime of weak or easterly zonal flow. Chu (1985) incorporated some consequences of the β effect in modeling the

Corresponding author address: Dr. Peter R. Bannon, Department of Meteorology, The Pennsylvania State University, 503 Walker Building, University Park, PA 16802-5013.

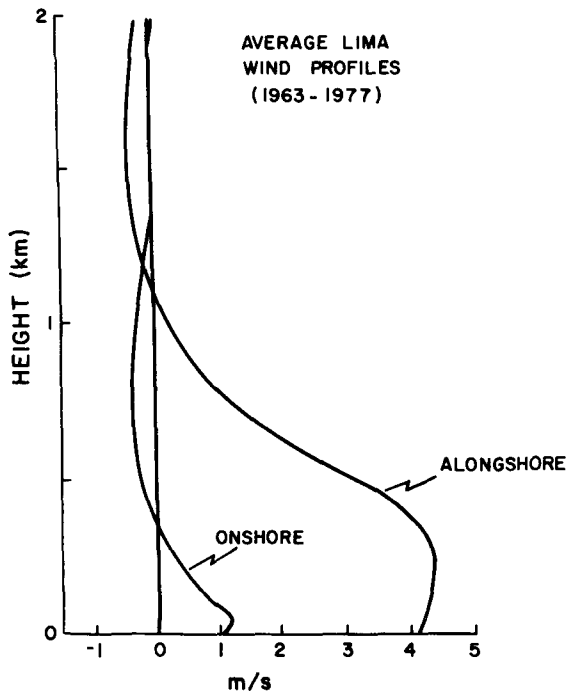

FIG. 1. Annual average of the vertical profiles of the onshore and alongshore wind (m s^{-1}) at Lima, Peru (after Enfield 1981).

transverse cross-coastal circulation of Chile and Peru but the alongshore flow was prescribed.

The purpose of this investigation is to model the low-level wind profile along the coastal desert using a boundary-layer model that includes the β effect. It is shown that the β effect is crucial for the presence of subsidence along the coast.

Section 2 describes the essential physics of the model and outlines the method of solution. Section 3 considers two special solutions that highlight the weaknesses of an f-plane solution. These cases are compared with the stably stratified Ekman layer model of Leetmaa (1978) and with the inviscid β-plane model of Stommel and Veronis (1957). Section 4 presents the solution of the general problem with sensitivity studies and applies the model to the flow over Lima. An Appendix extends the model physics to include a crude estimate of the role of cold air advection on the coastal flow. We conclude in section 5 with a discussion of our results, their limitations, and their implications for the maintenance of the coastal desert. The reader is referred to the work of Abreu (1991) for a more detailed discussion of many of the issues discussed here.

2. The model

a. *Model formulation*

This model studies the effects of nonuniform rotation on the steady circulation of a hydrostatic, Boussinesq, diffusive fluid subjected to a thermal contrast from below. For definiteness we consider a meridional coastal situation on the β plane with a cool ocean ($x < 0$) adjacent to a warm land surface ($x > 0$). Figure 2 summarizes the model geometry. The zonal, meridional, and vertical velocity components (u, v, w) are oriented conventionally in the x, y, and z directions, respectively. The Coriolis parameter is defined as

$$f(y) = f_0 + \beta y, \tag{2.1}$$

where f_0 and β are constants.

The flow consists of the sum of a resting basic state and a perturbation due to the zonal thermal gradient. The basic state is stably stratified with uniform buoyancy frequency N. The perturbation is assumed small so that linear dynamics hold. This assumption is consistent with the slow wind speeds (Fig. 1) of the region.

The fluid has constant vertical thermal and mechanical (eddy) diffusivities κ and η, respectively. The flow is therefore cooled from below over the ocean and warmed over the land; it also experiences dissipation due to bottom friction. Lateral diffusion of heat and momentum is ignored.

The linearized equations for the steady-state problem are

$$-fv = -\frac{\partial \phi}{\partial x} + \hat{\eta}\frac{\partial^2 u}{\partial z^2}, \tag{2.2}$$

$$+fu = -\frac{\partial \phi}{\partial y} + \eta\frac{\partial^2 v}{\partial z^2}, \tag{2.3}$$

$$\frac{\partial \phi}{\partial z} = b, \tag{2.4}$$

$$\frac{\partial u}{\partial x} + \frac{\partial v}{\partial y} + \frac{\partial w}{\partial z} = 0, \tag{2.5}$$

$$N^2 w = \kappa\frac{\partial^2 b}{\partial z^2}, \tag{2.6}$$

where ϕ is the geopotential and $b = g\theta/\theta_0$ is the buoyancy. Here θ is the perturbation of the potential temperature from its reference value, θ_0, and g is the acceleration due to gravity. In (2.2), the caret on the viscosity is used as a flag. Its importance is discussed below for the solution of the semigeostrophic problem.

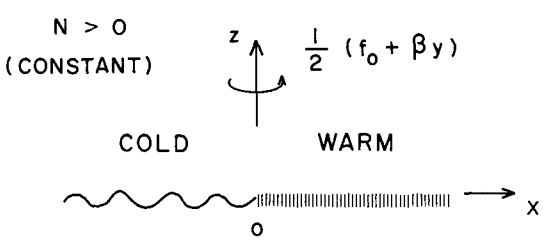

FIG. 2. Schematic diagram of the geometry of the model on a beta plane. Cold air lies to the west ($x < 0$) over the ocean, and warm air to the east ($x > 0$) over the land.

Equations (2.2)–(2.6) constitute a complete set of five equations for the five unknowns u, v, w, b, and ϕ. We note that the inclusion of a small constant Newtonian cooling in the thermodynamic equation does not significantly alter the results presented here.

b. Derivation of the governing equation

We cross differentiate (2.2) and (2.3) and use continuity (2.5) to obtain a vorticity equation in the form

$$\beta v = f\frac{\partial w}{\partial z} + \frac{\partial^2}{\partial z^2}\left(\eta\frac{\partial v}{\partial x} - \hat{\eta}\frac{\partial u}{\partial y}\right). \tag{2.7}$$

Rewriting the stretching term using the heat equation (2.6) yields

$$\beta v = \frac{f\kappa}{N^2}\frac{\partial^3 b}{\partial z^3} + \frac{\partial^2}{\partial z^2}\left(\eta\frac{\partial v}{\partial x}\right) - \frac{\partial^2}{\partial z^2}\left(\hat{\eta}\frac{\partial u}{\partial y}\right), \tag{2.8}$$

which relates the wind and buoyancy fields.

A generalized thermal wind relation provides a second relation between these two fields. Differentiation of (2.2) and (2.3) in the vertical and use of the hydrostatic relation (2.4) yields

$$-f\frac{\partial v}{\partial z} = -\frac{\partial b}{\partial x} + \hat{\eta}\frac{\partial^3 u}{\partial z^3}, \tag{2.9}$$

$$+f\frac{\partial u}{\partial z} = -\frac{\partial b}{\partial y} + \eta\frac{\partial^3 v}{\partial z^3}, \tag{2.10}$$

respectively. Multiplying (2.9) by f and substituting for the zonal wind from (2.10) produces the required relation,

$$\left(\eta\hat{\eta}\frac{\partial^4}{\partial z^4} + f^2\right)\frac{\partial v}{\partial z} = f\frac{\partial b}{\partial x} + \hat{\eta}\frac{\partial^2}{\partial z^2}\left(\frac{\partial b}{\partial y}\right). \tag{2.11}$$

We note that (2.11) reduces to an Ekman balance if there are no horizontal variations and to a thermal wind balance if $\hat{\eta}$ vanishes.

The anisotropic structure of the flow can be used to simplify the pair (2.8) and (2.11). Typically the meridional scale, L_y, of the flow is much larger than the zonal scale, L_x (e.g., Oort 1983), and the scale of the alongshore flow, V, is stronger than the cross-coastal flow, U (see Fig. 1). This structure implies that the contribution of the alongshore flow dominates the relative vorticity:

$$\frac{\partial u}{\partial y} \ll \frac{\partial v}{\partial x}, \tag{2.12a}$$

and that the cross-coastal gradient of buoyancy dominates the alongshore gradient so that:

$$\hat{\eta}\frac{\partial^2}{\partial z^2}\left(\frac{\partial b}{\partial y}\right) \ll f\frac{\partial b}{\partial x}. \tag{2.12b}$$

The scale of the ratio of the left-hand-side terms to those on the right in (2.12) is

$$\frac{\partial u/\partial y}{\partial v/\partial x} \sim \left(\frac{U}{V}\right)\left(\frac{L_x}{L_y}\right) \sim 0.025 \ll 1$$

and

$$\frac{\hat{\eta}\partial^2(\partial b/\partial y)/\partial z^2}{f\partial b/\partial x} \sim \left(\frac{\eta}{fD^2}\right)\left(\frac{L_x}{L_y}\right) \sim 0.04 \ll 1$$

where we have chosen $L_x = 200$ km, $L_y = 2000$ km, $U = 1$ m s^{-1}, $V = 4$ m s^{-1}, $\eta = 5$ m^2 s^{-1}, $f = -5 \times 10^{-5}$ s^{-1}, and $D = 500$ km is the characteristic depth of the flow. Thus, with the assumptions (2.12), the last terms in (2.8) and (2.11) can be ignored and we have

$$\beta v = \frac{f\kappa}{N^2}\frac{\partial^3 b}{\partial z^3} + \frac{\partial^2}{\partial z^2}\left(\eta\frac{\partial v}{\partial x}\right), \tag{2.13}$$

and

$$\left(\eta\hat{\eta}\frac{\partial^4}{\partial z^4} + f^2\right)\frac{\partial v}{\partial z} = f\frac{\partial b}{\partial x}, \tag{2.14}$$

which represent two equations for v and b.

Solving for b we obtain the governing equation for the perturbation buoyancy field in the form

$$\frac{\eta\hat{\eta}}{f^2}\frac{\partial^8 b}{\partial z^8} + \frac{\partial^4 b}{\partial z^4} + \frac{\eta N^2}{\kappa f^2}\frac{\partial^2}{\partial x^2}\left(\frac{\partial^2 b}{\partial z^2}\right) - \frac{\beta N^2}{\kappa f^2}\frac{\partial b}{\partial x} = 0. \tag{2.15}$$

This partial differential equation is eighth order in z but second order in x. Since there are no meridional derivatives, the y dependence enters parametrically in (2.15) and we solve (2.15) assuming $f = f_0$ is constant. This approach allows us to treat this fundamentally three-dimensional problem in a two-dimensional context.

c. Boundary conditions

The model atmosphere is vertically semi-infinite with a flat rigid lower boundary at $z = 0$. We assume that all fields remain bounded in the vertical as $z \to \infty$. At the lower boundary we prescribe the buoyancy (i.e., temperature) perturbation to be a function of x only. The kinematic boundary condition requires that the vertical velocity vanish at $z = 0$. For the horizontal flow we follow Taylor (1915) and assume that the surface stress is in the direction of the wind. Mathematically, the lower boundary conditions are

$$b(x, y, 0) = b_0(x), \tag{2.16}$$

$$w(x, y, 0) = 0, \tag{2.17}$$

$$Cu = \frac{\partial u}{\partial z}, \tag{2.18}$$

$$Cv = \frac{\partial v}{\partial z}, \tag{2.19}$$

where the constant $C = 2 \times 10^{-3}$ m^{-1} is obtained by

equating the eddy and linearized bulk aerodynamic formulations for the surface stress. Alternatively, letting $C = \infty$ yields the no-slip conditions

$$u(z = 0) = 0, \quad v(z = 0) = 0. \tag{2.20}$$

Horizontally the model atmosphere has a finite zonal domain such that $-L \leq x \leq L$. All flow variables are assumed to be periodic in x.

d. Solution

We solve (2.15) analytically using the Fourier transform technique. Let the surface buoyancy perturbation take the form

$$b_0(x) = b_{00}e^{ikx}, \tag{2.21}$$

where b_{00} is a constant and k is a zonal wavenumber with an integral number of wavelengths over the domain $2L$. Then (2.15) has a solution of the form

$$b(x, z) = e^{ikx} \sum_{j=1}^{J} A_j e^{-\lambda_j z}, \tag{2.22}$$

where $A_j = A_j(k)$ are dimensional constants.

Here $\lambda_j = \lambda_j(k)$ represent vertical decay rates that are solutions of

$$\frac{\eta\hat{\eta}}{f_0^2}\lambda^8 + \lambda^4 - \left(\frac{\eta k^2 N^2}{\kappa f_0^2}\right)\lambda^2 - \frac{ik\beta N^2}{\kappa f_0^2} = 0. \tag{2.23}$$

In writing (2.23) we have evaluated (2.15) at $y = 0$. This eighth-order polynomial with constant coefficients is solved numerically. We select only the roots that have positive real parts in order to satisfy the boundedness conditions at $z = \infty$. Therefore, the summation in (2.22) and related equations is over these decaying disturbances. Typically $J \leq 4$. Then the constants A_j are determined by the vertical boundary conditions (2.16)–(2.19) in a straightforward manner.

We obtain solutions of the other flow variables as follows. The hydrostatic equation implies

$$\phi(x, z) = -e^{ikx} \sum_{j=1}^{j} \frac{A_j}{\lambda_j} e^{-\lambda_j z}. \tag{2.24}$$

Note that the buoyancy and the geopotential fields are independent of y:

$$\frac{\partial b}{\partial y} = 0, \quad \frac{\partial \phi}{\partial y} = 0. \tag{2.25}$$

The former result indicates that the assumption (2.12b) is satisfied a posteriori. Use of the latter simplifies the meridional momentum equation (2.3) to

$$fu = +\eta \frac{\partial^2 v}{\partial z^2}. \tag{2.26}$$

Expressions for the velocity field follows from (2.22), (2.14), (2.26), and (2.6). We find

$$v(x, y, z) = -\frac{ik}{f} e^{ikx} \sum_{j=1}^{J} B_j e^{-\lambda_j z}, \tag{2.27}$$

$$u(x, y, z) = -\frac{ik\eta}{f^2} e^{ikx} \sum_{j=1}^{J} \lambda_j^2 B_j e^{-\lambda_j z}, \tag{2.28}$$

$$w(x, y, z) = \frac{\kappa}{N^2} e^{ikx} \sum_{j=1}^{J} \lambda_j^2 A_j e^{-\lambda_j z}, \tag{2.29}$$

where

$$B_j = A_j \Big/ \left[\lambda_j\left(\frac{\lambda_j^4 \eta\hat{\eta}}{f_0^2} + 1\right)\right]. \tag{2.30}$$

Note that the Coriolis parameter in (2.27) and (2.28) is given by (2.1) and is nonconstant. It can be shown that the solution for the velocity fields satisfies the three-dimensional continuity equation (2.5). This important result indicates that the divergence of the meridional wind can contribute to the vertical motion field and that evaluation of (2.15) at $y = 0$ is internally consistent with the solutions (2.27)–(2.29). Note that the importance of the divergence of the meridional wind is not inconsistent with the scaling arguments for (2.12a), which apply to the vorticity field.

A surface thermal anomaly of the form

$$\theta(x, z = 0) = \frac{T_0}{(\pi/2)} \tan^{-1}(x/a) \tag{2.31}$$

is used to represent the coastal contrast mathematically. Here T_0 is a measure of the amplitude of the land–sea contrast while a is a measure of its horizontal scale. We choose $T_0 = 5$ K and $a = 200$ km. All solutions vary linearly with the amplitude T_0.

The origin of the β plane is taken to be at 12°S, corresponding to the observations for Lima. Thus, $f_0 = -3.03 \times 10^{-5}\ \mathrm{s}^{-1}$ and $\beta = 2.24 \times 10^{-11}\ \mathrm{m}^{-1}\ \mathrm{s}^{-1}$. Application of the results to the Northern Hemisphere only requires that positive meridional velocities be interpreted as being equatorward. Other parameter settings are $N^2 = 1.2 \times 10^{-4}\ \mathrm{s}^{-2}$, $g = 9.8\ \mathrm{m\ s}^{-2}$, $\theta_0 = 290$ K, and $\eta = \kappa = 5\ \mathrm{m}^2\ \mathrm{s}^{-1}$. The sensitivity of the results to these parameter settings is examined in section 4c.

The solution for the forcing (2.31) is obtained using the fast Fourier transform technique. In this approach the total solution is the sum of the solutions [(2.22), (2.27)–(2.29)] for each sinusoidal mode in a Fourier series expansion of (2.31). A total of 512 points cover the zonal domain of 6400 km for a resolution of 12.5 km. To handle the Gibbs phenomenon (e.g., Arfken 1966) associated with using (2.31) over a finite domain, we apply a decaying function to (2.31) beyond $|x| > 2300$ km to smooth the field to zero at the ends of the domain. This smoothing also helps to eliminate oscillations associated with the derivative of a Fourier transform (Lanczos 1956).

3. Special cases

We first discuss two special cases of the problem posed by the governing equation (2.15) before presenting results for the general case in section 4. The discussion of these two cases, the f-plane and the semigeostrophic β-plane solutions, provides valuable insight into the general solution. Because these special cases display several deficiencies, we postpone an examination of the sensitivity of the results to section 4.

a. The f-plane solution

The model equations (2.2)–(2.6) on the f plane can be solved exactly assuming no meridional variation. We find

$$\frac{\eta\hat{\eta}}{f_0^2}\frac{\partial^8 b}{z^8}+\frac{\partial^4 b}{\partial z^4}+\frac{\eta N^2}{\kappa f_0^2}\frac{\partial^2}{\partial x^2}\left(\frac{\partial^2 b}{\partial z^2}\right)=0. \quad (3.1)$$

This result also follows by making the f-plane approximation in (2.15). The corresponding equation for the vertical decay rates is

$$\frac{\eta\hat{\eta}}{f_0^2}\lambda^8+\lambda^4-\left(\frac{\eta k^2 N^2}{\kappa f_0^2}\right)\lambda^2=0. \quad (3.2)$$

The three nonzero vertically decaying solutions of (3.2) are plotted in Fig. 3 as a function of the zonal wavenumber k for the parameter settings given at the end of section 2 with $\beta = 0$ and $\hat{\eta} = \eta$.

The solution of (3.2) for the zonally symmetric case ($k = 0$) yields the pure Ekman roots for a bounded solution,

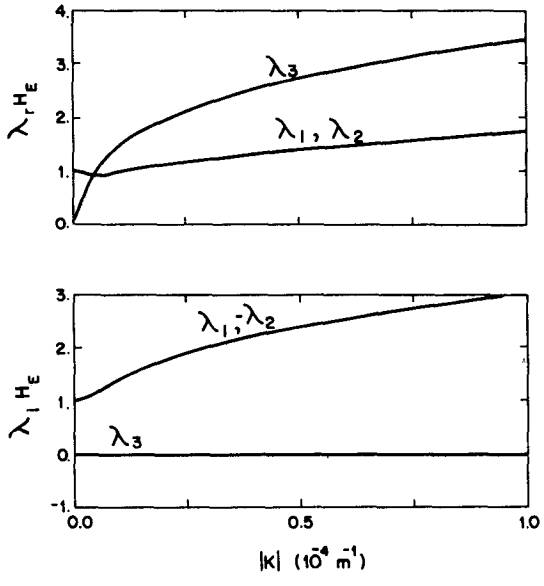

FIG. 3. Real (a) and imaginary (b) part of the vertical decay rate λ as a function of the zonal wavenumber, k, for the f-plane solution. The decay rate is scaled by the Ekman rate $(1/H_E)$.

$$\lambda_E=\left(\frac{|f_0|}{2\eta}\right)^{1/2}(1\pm i). \quad (3.3)$$

We find it convenient to normalize the roots in Fig. 3 and subsequent plots by the Ekman scale:

$$H_E=\left(\frac{2\eta}{|f_0|}\right)^{1/2}=(\mathrm{Re}\lambda_E)^{-1}. \quad (3.4)$$

The Ekman roots λ_1 and λ_2 form a complex conjugate pair. They generally display larger amplitudes for nonzero k. Note that (3.3) is also the solution of (3.2) for the case of nonzero k but neutral stability (i.e., $N^2 = 0$). Thus, the Ekman layer is typically shallower and has a tighter spiral in the presence of stable stratification. This confinement of the Ekman layer is not due to the suppression of turbulence by the stratification since the eddy diffusivities in the present model are prescribed and are not functions of the stability. Rather the confinement arises from dynamical adjustments (e.g., Leetmaa 1971).

A third real positive root of (3.2) is also present for nonzero k. Lineykin (1955) first introduced this root in its pure form by assuming a geostrophic meridional wind. Then $\hat{\eta} = 0$ [see (2.2)] in (3.1) and the solution is

$$\lambda_L=\left(\frac{\eta}{\kappa}\frac{N^2k^2}{f_0^2}\right)^{1/2}. \quad (3.5)$$

This root grows linearly in k (see Fig. 3) until the wind shear is sufficiently large that the vertical diffusion of momentum becomes important and the thermal wind balance is invalid. Fig. 3 suggests this linear dependency occurs for $\lambda_3 \leqslant \mathrm{Re}(\lambda_E)$. Subsequent growth of the root with increasing k is at a reduced rate. For a Prandtl number of unity (i.e., $\eta = \kappa$), the depth scale of the Lineykin root corresponds to the Rossby height (Gill 1982).

Two additional roots of (3.2) are the trivial solutions

$$\lambda_C = 0 \quad \text{and} \quad 0, \quad (3.6)$$

which Leetmaa (1971) and Mahrt (1980) label the Couette solution since it corresponds to a linear buoyancy profile

$$b_C = C_1 z + C_2, \quad (3.7)$$

where C_1 and C_2 are constants. Such a solution can not satisfy the boundedness condition at infinity. (Note that while $b_C = C_2$ is bounded, the thermal wind relation implies an unbounded velocity field.) Leetmaa (1971) presents solutions including the Couette component for a fluid of finite depth.

Assuming a semi-infinite atmosphere, we dismiss the Couette components and seek a solution with only three roots [$J = 3$ in (2.22)]. We must, however, relax the boundary conditions (2.16)–(2.19) since not all four conditions can now be satisfied simultaneously. Figure 4 shows the f-plane solution for (2.31) if we

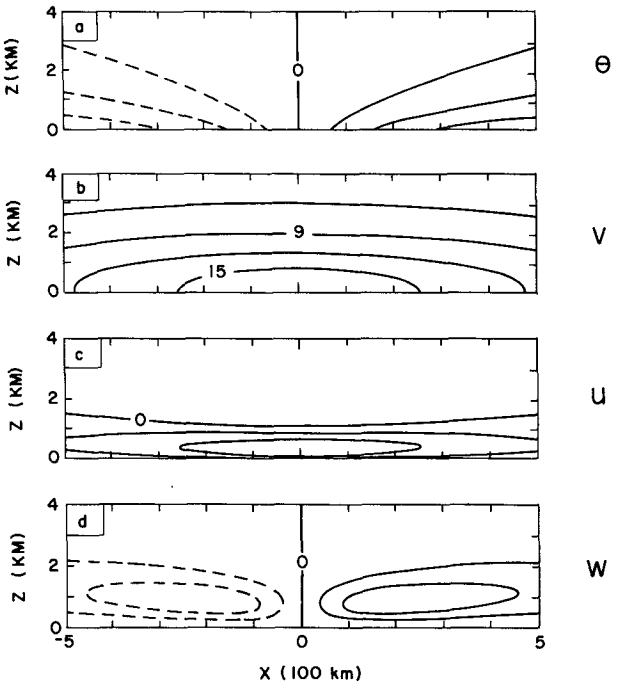

FIG. 4. Contour plot of the perturbation fields, θ, v, u, and w near the coast for the f-plane solution. The contour intervals are 1 K, 3 m s^{-1}, 0.5 m s^{-1}, and 0.5 mm s^{-1} in (a), (b), (c), and (d), respectively. Negative contours are dashed.

satisfy the kinematic, thermal, and zonal no-slip conditions [(2.16), (2.17), and (2.18) with $C = \infty$] but permit the meridional wind to exhibit slip along the lower boundary. This choice is motivated by an attempt to model the observations of Fig. 1.

The solution displays a thermally direct circulation with warm air rising over the land and cold air sinking over the ocean. The cross-coastal winds are onshore at low levels and offshore aloft. This result is consistent with Fig. 1 but the alongshore flow of Fig. 4 is too strong and does not exhibit a flow reversal aloft.

b. *Semigeostrophic β-plane solution*

We now make the semigeostrophic approximation that the alongshore wind is geostrophic but retain the β-plane approximation. Then $\hat{\eta} = 0$ in (2.2) and the governing equation (2.15) and the λ equation (2.23) reduce to

$$\frac{\partial^4 b}{\partial z^4} + \frac{\eta N^2}{\kappa f^2}\frac{\partial^2}{\partial x^2}\left(\frac{\partial^2 b}{\partial z^2}\right) - \frac{\beta N^2}{\kappa f^2}\frac{\partial b}{\partial x} = 0, \quad (3.8)$$

and

$$\lambda^4 - \left(\frac{\eta N^2 k^2}{\kappa f_0^2}\right)\lambda^2 - \frac{ik\beta N^2}{\kappa f_0^2} = 0, \quad (3.9)$$

respectively.

The complex quadratic equation (3.9) for λ^2 has the solution

$$\lambda_{SG} = +\left\{\left(\frac{\eta}{2\kappa}\frac{N^2k^2}{f_0^2}\right)\left[1 \pm \left(1 + \frac{4i\beta\kappa f_0^2}{\eta^2 N^2 k^3}\right)^{1/2}\right]\right\}^{1/2}. \quad (3.10)$$

The two decaying roots of (3.10) are plotted in Fig. 5 for the parameter settings of section 2. Both roots are complex. The larger of the two, λ_{SG1}, satisfies (3.10) with the positive sign. This root represents a Lineykin solution distorted by the β effect. Mathematically one can show that

$$\lim_{k\to\infty}\lambda_{SG1} = \lambda_L, \quad \lim_{\beta\to 0}\lambda_{SG1} = \lambda_L. \quad (3.11)$$

For large k, the second term in (3.9) dominates the last term and a balance exists between the first two terms.

Stommel and Veronis (1957) consider an inviscid but thermally diffusive fluid on the β plane and find

$$\frac{\partial^4 b}{\partial z^4} - \frac{\beta N^2}{\kappa f^2}\frac{\partial b}{\partial x} = 0, \quad (3.12)$$

which can be obtained from (2.15) or (3.8) by letting $\hat{\eta} = \eta = 0$. The corresponding roots are

$$\lambda_{SV1,2} = \left(\frac{\beta k N^2}{\kappa f_0^2}\right)^{1/4}(e^{i\pi/8}, e^{-3i\pi/8}), \quad (3.13)$$

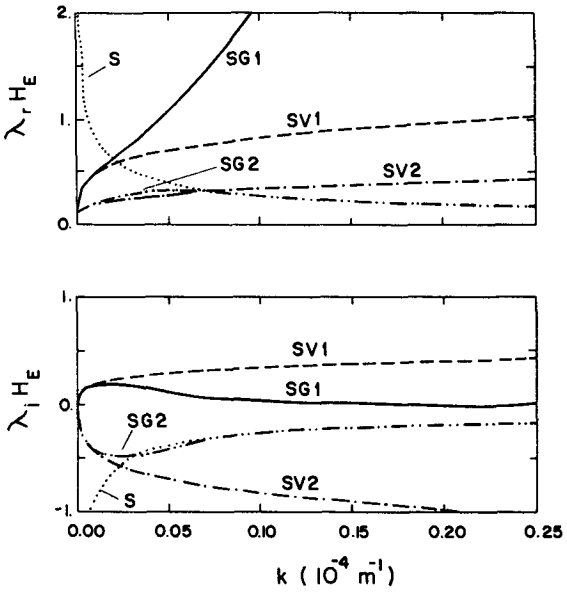

FIG. 5. Real (a) and imaginary (b) part of the vertical decay rate λ as a function of the zonal wavenumber, k, for the semigeostrophic β-plane solution. The decay rate is scaled by the Ekman rate ($1/H_E$). The semigeostrophic roots are solid and dot-dot-dashed. The Stommel–Veronis roots are dashed and dot-dashed, while the Sverdrup root is dotted. Roots for negative k are the complex conjugate of the root for positive k.

and appear in Fig. 5 as dashed lines. This figure indicates that the semigeostrophic roots agree with those of (3.13) for small k. This finding is consistent with (3.9) since, in the limit of small k, the second term may be ignored compared with the third term to yield the roots (3.13).

Inspection of Fig. 5 also indicates that the Stommel–Veronis balance (3.12) is invalid for large k where $\lambda_{SG2} \to 0$. In such a case, we may ignore the first term in (3.8) to obtain

$$\eta \frac{\partial^2}{\partial x^2}\left(\frac{\partial^2 b}{\partial z^2}\right) - \beta \frac{\partial b}{\partial x} = 0, \tag{3.14}$$

which implies the decaying root

$$\lambda_S = \left(\frac{\beta}{\eta k}\right)^{1/2} e^{-i\pi/4}. \tag{3.15}$$

Figure 5 plots λ_S as a dotted line; it is clearly seen that $\lambda_{SG2} \to \lambda_S$ for $k \geq 5 \times 10^{-6}$ m^{-1}. Thus, $\lambda_{SG2} \to \lambda_S \to 0$ for large horizontal wavenumber while $\lambda_{SG1} \to \lambda_L \to \infty$.

We note that (3.14) can be derived from (2.15) by considering a viscous but thermally nondiffusive fluid on the β plane and letting κ tend to zero. The corresponding vorticity equation in this case is

$$\beta v = \eta \frac{\partial^2}{\partial z^2}\left(\frac{\partial v}{\partial x}\right), \tag{3.16}$$

which represents a Sverdrup balance in which the curl of the frictional force leads to meridional advection of the planetary vorticity.

Comparison of (3.8) and (3.9) with (3.1) and (3.2) indicates that the Ekman balance has been eliminated and the buoyancy equation has been reduced to fourth-order in z. Thus, it is not possible to satisfy the dynamic boundary conditions (2.18) and (2.19). The solution of (3.8) satisfying only the thermal and kinematic conditions (2.16) and (2.17) appears in Fig. 6 and displays many intriguing features. The relatively strong alongshore wind has a surface maximum almost 100 km offshore and reverses direction aloft. The cross-coastal flow is offshore and relatively deep but is much weaker than the alongshore component. Both wind components display slip at the surface, as expected, and there is no Ekman layer. The vertical motion field displays subsidence both offshore and inland. This subsidence, due in part to the divergence of the meridional wind, produces warm anomalies aloft over the coastal region by adiabatic warming. As a consequence, the static stability is enhanced near the coast.

The striking features of the solution displayed in Fig. 6 arise from the beta effect, which allows for the existence of Rossby waves. For a nondiffusive fluid, Rossby waves propagating their energy upward display (e.g., see Gill 1982, p. 524) a westward phase tilt with height, warm air flowing poleward, and subsidence and westward ageostrophic flow along the pressure trough. Such

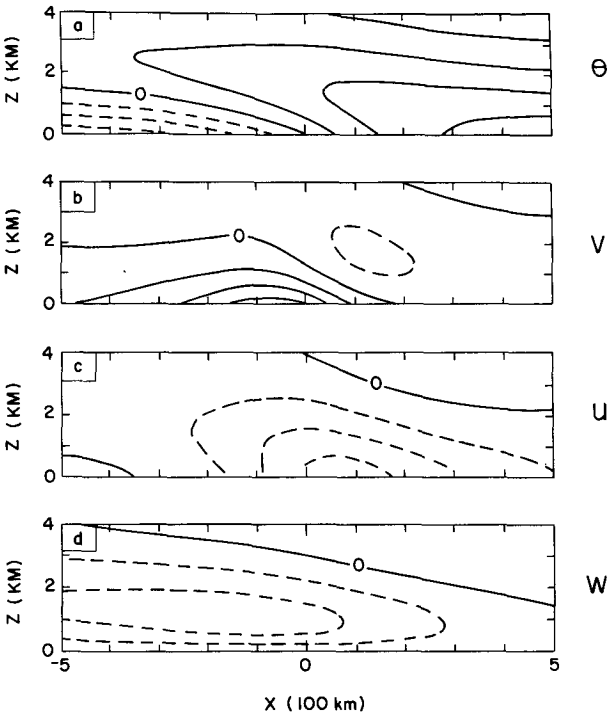

FIG. 6. Contour plot of the perturbation fields θ, v, u, and w near the coast for the semigeostrophic β-plane solution. The contour intervals are 1 K, 5 m s^{-1}, 0.5 m s^{-1}, and 1.0 mm s^{-1} in (a), (b), (c), and (d), respectively. Negative contours are dashed.

a wave can be stationary in the presence of a mean eastward wind when vortex stretching and relative vorticity advection balance the advection of planetary vorticity. The present model considers a diffusive fluid with no mean wind. In this situation a stationary Rossby wave exists for which the advection of planetary vorticity is balanced by either the mechanical diffusion of momentum [see (3.16)] in the Sverdrup limit or vortex stretching,

$$\beta v = f_0 \frac{\partial w}{\partial z}, \tag{3.17}$$

in the Stommel–Veronis limit or both. Here the adiabatic warming/cooling associated with any vortex stretching is balanced by thermal diffusion [see (2.6)] rather than by the thermal advection for the nondiffusive Rossby wave. Thus, the solution depicted in Fig. 6 represents the Fourier sum of forced diffusive Rossby waves generated by the imposed surface temperature gradient. These waves tilt westward with height but decay vertically rather than being free to propagate.

c. *Summary*

Analysis of two special cases of the general problem has lead to consideration of four physically distinct solutions (see Table 1). The Ekman and Sverdrup solutions represent mechanical balances, while those of

TABLE 1. Summary of the major features of the idealized solutions.

Ekman	Lineykin	Sverdrup	Stommel–Veronis
Momentum equation:			
$-f_0\mathbf{k}\times\mathbf{v}=\eta\dfrac{\partial^2 v}{\partial z^2}$	$f_0\dfrac{\partial v}{\partial z}=\dfrac{\partial b}{\partial x}$	$-f_0\mathbf{k}\times\mathbf{v}=\eta\dfrac{\partial^2 v}{\partial z^2}$	$f\dfrac{\partial v}{\partial z}=\dfrac{\partial b}{\partial x}$
Vorticity equation:			
—	$0=f_0\dfrac{\partial w}{\partial z}+\eta\dfrac{\partial^2}{\partial z^2}\left(\dfrac{\partial v}{\partial x}\right)$	$\beta v=\eta\dfrac{\partial^2}{\partial z^2}\left(\dfrac{\partial v}{\partial x}\right)$	$\beta v=f_0\dfrac{\partial w}{\partial z}$
Heat equation:			
—	$N^2 w=\kappa\dfrac{\partial^2 b}{\partial z^2}$	—	$N^2 w=\kappa\dfrac{\partial^2 b}{\partial z^2}$
Depth scale:			
$H_E=\left(\dfrac{2\eta}{\lvert f_0\rvert}\right)^{1/2}$	$H_L=\left(\dfrac{\kappa f_0^2}{\eta N^2 k^2}\right)^{1/2}$	$H_S=\left(\dfrac{\eta k}{\beta}\right)^{1/2}$	$H_{SV}=\left(\dfrac{\kappa f_0^2}{\beta k N^2}\right)^{1/4}$

Lineykin and of Stommel and Veronis are primarily thermomechanical. Each solution can also be represented as a balance between two of the terms in the buoyancy equation:

$$\overbrace{\frac{\eta\hat{\eta}}{f^2}\frac{\partial^8 b}{\partial z^8}}^{\text{Ekman}}+\overbrace{\underbrace{\frac{\partial^4 b}{\partial z^4}}_{\text{Stommel and Veronis}}+\frac{\eta N^2}{\kappa f^2}\frac{\partial^2}{\partial x^2}\left(\frac{\partial^2 b}{\partial z^2}\right)}^{\text{Lineykin}}-\overbrace{\underbrace{\frac{\beta N^2}{\kappa f^2}\frac{\partial b}{\partial x}}_{\text{Stommel and Veronis}}}^{\text{Sverdrup}}=0. \tag{3.18}$$

While other balances are mathematically possible, these four appear to be the most relevant physically.

We note that each of the two special cases has failed to provide a realistic solution to the problem. The Couette degeneracy of the f-plane case prevented satisfying all four boundary conditions at the ground. Further, the f-plane solution lacks the observed meridional flow reversal aloft. The semigeostrophic β-plane case has eliminated the Couette degeneracy. Its flow reverses aloft but contains no Ekman layer dynamics. The deficiencies of these two special cases are removed in the next section where the general solution is presented.

4. General solution

This section presents the bounded solution of the governing equation (2.15) subject to the lower boundary conditions (2.16)–(2.19). We first examine the roots of the eighth-order polynomial (2.23) and then display the solution for the surface thermal anomaly (2.31). We compare these results with the special cases of the preceding section. A third subsection summarizes the sensitivity of the model to variations in the input parameters. We then apply this knowledge to the specific case of the coastal flow near Lima in the last subsection.

a. *Roots of the polynomial (2.23)*

The vertically decaying roots of the polynomial (2.23) are plotted in Fig. 7 for the parameter settings given at the end of section 2. We first note that there are four nonzero roots; thus, the Couette degeneracy of the f-plane solution has been eliminated by the inclusion of the β effect. Mathematically this result arises from the inclusion of the last term in (2.23).

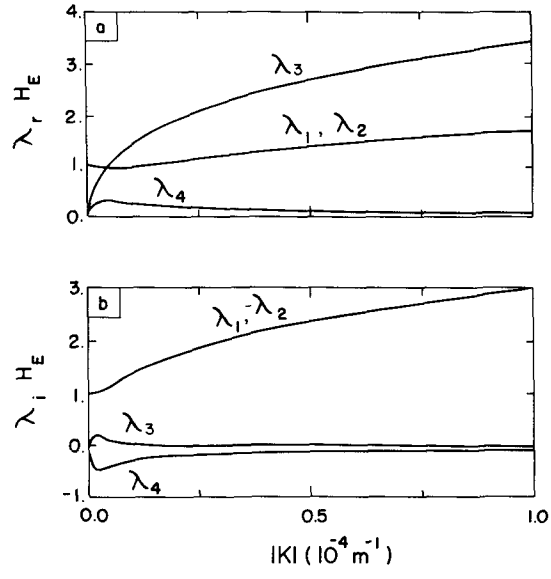

FIG. 7. Real (a) and imaginary (b) part of the vertical decay rate λ as a function of the zonal wavenumber, k, for the general solution. The decay rate is scaled by the Ekman rate ($1/H_E$). Roots for negative k are the complex conjugate of the root for positive k.

Comparison of Figs. 3, 5, and 7 indicates the following features. One pair of roots, λ_1 and λ_2, correspond to the stratified Ekman roots. While they no longer form an exact complex conjugate pair as they did for the f-plane case, they are relatively unaltered by the β effect. The second pair, λ_3 and λ_4, correspond approximately to the semigeostrophic roots (3.10). For small values of the wavenumber k, $\lambda_3 \sim \lambda_{SG1}$. For larger values, this root behaves more like the modified Lineykin root, λ_3, of the f-plane case. Note that here, unlike in the f-plane case, the λ_3 root has a positive imaginary part. The fourth root, λ_4, behaves like the second semigeostrophic root, λ_{SG2}, which is an amalgam of a Stommel–Veronis balance for small k and a Sverdrup balance for large k.

b. A solution

Figure 8 presents contour plots of the fields for a surface thermal anomaly of the form (2.31) subject to the boundary conditions (2.16)–(2.19). The cross-coastal flow is onshore below 1 km with a maximum at the coast of 5 m s^{-1}. A weaker offshore return flow exists from 1 to 3 km. The alongshore flow is equatorward near the surface with a maximum off the coast over the water. This flow reverses above about 1.5 km to become weakly poleward. The air is subsiding both over the ocean and at the coast. Consequently, the thermal field exhibits a coastal intensification of the static stability. These features of the general solution represent a combination of those of the two special cases of the preceding section. The f-plane Ekman–Lineykin solution, with its relatively small vertical scale (i.e., large λ), tends to dominate near the surface while the semigeostrophic β-plane behavior of diffusive Rossby waves dominates aloft.

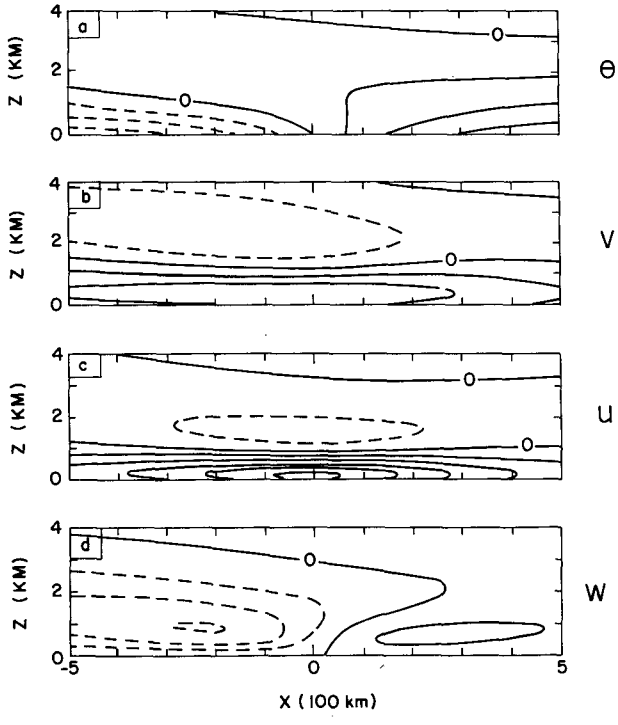

FIG. 8. Contour plot of the perturbation fields θ, v, u, and w near the coast for the general solution. The contour intervals are 1 K, 1 m s^{-1}, 0.5 m s^{-1}, and 1.0 mm s^{-1} in (a), (b), (c), and (d), respectively. Negative contours are dashed.

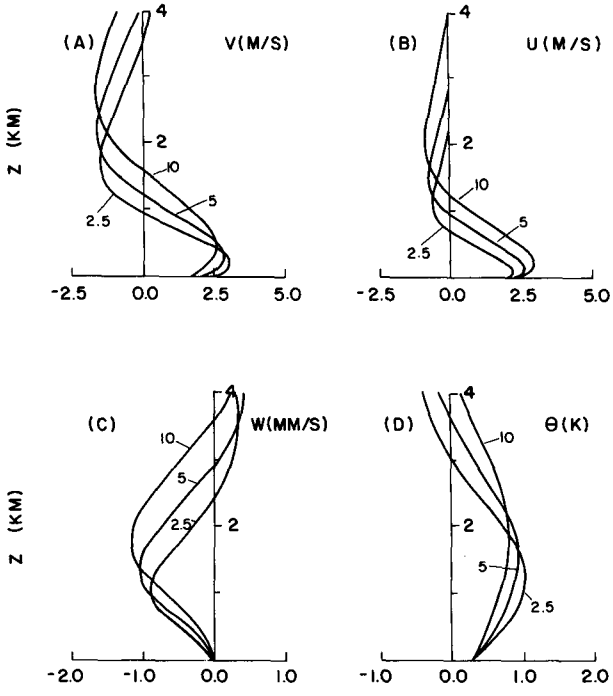

FIG. 9. Vertical profiles of the perturbation fields at the coastal station for the general solution for various values of the diffusivity labeled in units of m^2 s^{-1}. The Prandtl number is unity.

c. Sensitivity studies

We next examine the sensitivity of the general solution to changes in the parameter settings, many of which are poorly known. For convenience we plot vertical profiles of u, v, w, and θ at the grid point 18.75 km inland from the coast, henceforth referred to as the coastal station. Figure 9 displays the profiles for three different values of the diffusivity: $\eta = 2.5$, 5.0, and 10.0 m^2 s^{-1}. In each case the Prandtl number (Pr $= \eta/\kappa$) is unity. It is seen that an increase in the diffusivity leads to a deeper response with stronger u and w fields but weaker v and θ fields. We note that a larger thermal diffusivity enables the thermal anomaly to penetrate deeper into the fluid. This behavior is demonstrated in Fig. 10 where coastal profiles are shown for three values of the thermal diffusivity, $\kappa = 2.5$, 5.0, and 10.0 m^2 s^{-1}, while the mechanical diffusivity remains fixed at the reference value $\eta = 5$ m^2 s^{-1}. The solutions are weakly dependent on the diffusivity. For example, the characteristic depth scales of Table 1 are proportional to either the square or fourth root of η or κ.

We note that Fig. 10 also documents the sensitivity

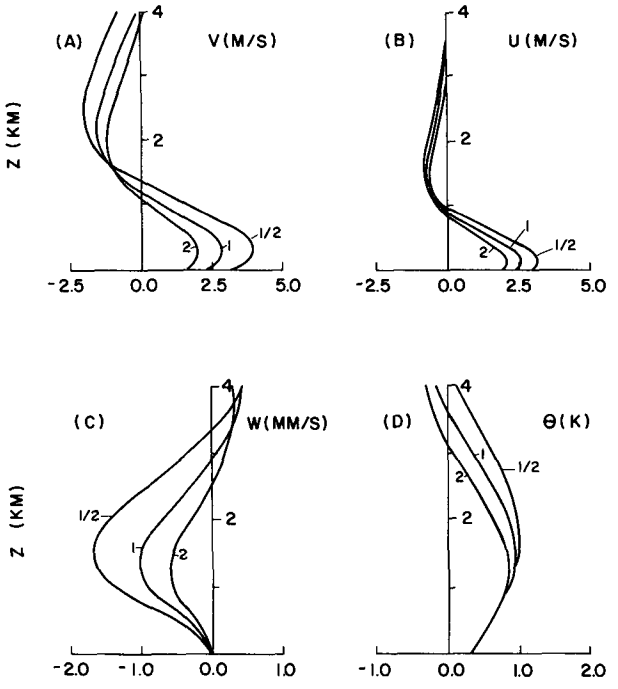

FIG. 10. Vertical profiles of the perturbation fields at the coastal station for the general solution for various values of the Prandtl number ($\Pr = = \eta/\kappa$). The mechanical diffusivity is fixed at $\eta = 5\ m^2\ s^{-1}$.

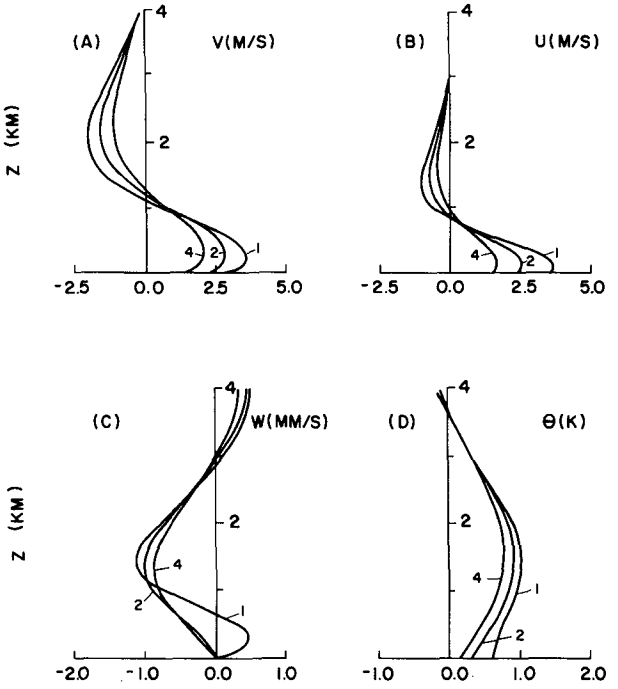

FIG. 11. Vertical profiles of the perturbation fields at the coastal station for the general solution for various values of the width, a, of the thermal coastal anomaly labeled in units of 100 km.

of the solution to changes in the ambient stratification. Inspection of (2.15) reveals that doubling N^2 has the same effect as halving κ. This behavior arises from the simplified heat balance (2.6).

Figure 11 documents the effect of changing the characteristic width a of the surface thermal anomaly (2.31). A broader anomaly leads to a weaker circulation, consistent with a decrease in the thermal gradient. For a sufficiently sharp coastal zone (e.g., $a = 100$ km) there can be rising motion below 1 km at the coastal station with subsidence dominating aloft.

d. Application to Lima, Peru

Observations (Fig. 1) indicate that the onshore flow is quite weak and shallow while the equatorward flow is stronger and deeper. To model this structure we set $\eta = 1\ m^2\ s^{-1}$ to reduce the depth of the Ekman layer. We also take $\kappa = 8\ m^2\ s^{-1}$. This small Prandtl number is consistent with an unstable, convectively driven boundary layer (e.g., Panofsky and Dutton 1984, p. 144). We note that the observations have a daytime bias, being the average of data from 1900 local time. For the surface temperature field (2.31) we set $T_0 = 3$ K and $a = 200$ km. This choice implies a total land–sea thermal contrast of 6 K, which is typical of the region (e.g., Enfield 1981; Prohaska 1973). The choice $a = 200$ km is a representative scale for the flow.

Figures 12 and 13 document the structure of the flow in this case. The wind profiles along the coast (Fig. 12) are in good agreement with observations. The weak onshore flow lies below 500 m with a deeper but still weaker flow aloft. The equatorward flow is deeper ($\sim$1 km thick) with a higher, stronger jet maximum of 4 m s^{-1} near 400 m. The predicted poleward flow aloft is stronger than observed. The horizontal structure of the flow (Fig. 13) includes an alongshore wind maximum located off the coast over the water, enhanced static stability near the coast, and low-level subsidence extending several hundred kilometers inland.

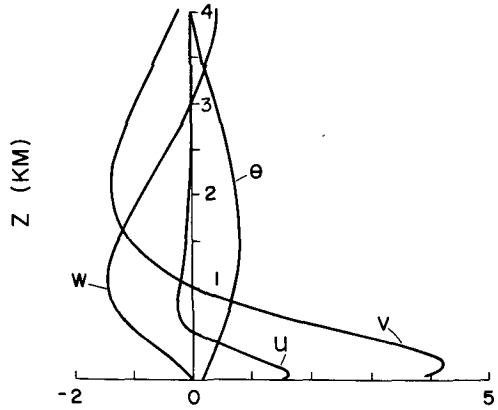

FIG. 12. Vertical profile of the perturbation fields at the coastal station for the model simulation of Lima, Peru (units of the abscissa: m s^{-1} for u and v, mm s^{-1} for w, and K for θ).

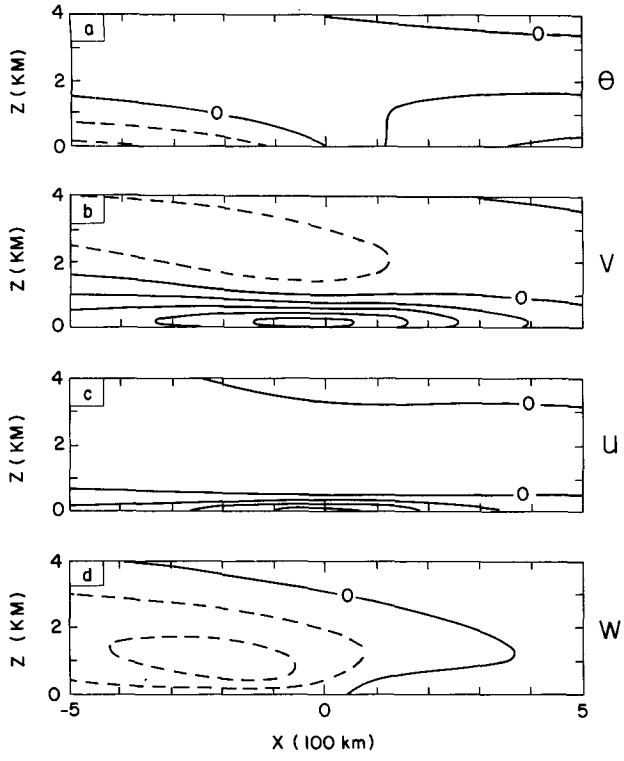

FIG. 13. Contour plot of the perturbation fields θ, v, u, and w near the coast for the model simulation of Lima, Peru. The contour intervals are 1 K, 1 m s^{-1}, 0.5 m s^{-1}, and 1.0 mm s^{-1} in (a), (b), (c), and (d), respectively. Negative contours are dashed.

5. Conclusions

We have developed a linear boundary-layer model on a β plane to explain some of the climatological features of the South American coastal desert. We assume a Boussinesq, stably stratified flow associated with a zonal thermal contrast at the surface. We also allow the flow to experience both heat diffusion and dissipation due to bottom friction. The resulting governing equation for the buoyancy field is a homogeneous eighth-order one in which the y dependence enters parametrically. Therefore, it is possible to solve this three-dimensional problem in a two-dimensional setting.

An analysis of the solutions indicates that there are four main balances (see Table 1) in the problem:

- An Ekman balance among the Coriolis, pressure gradient, and frictional forces. For the parameter settings in this paper (see section 2), the depth scale is $H_E \approx 600$ m.
- A Lineykin balance in which adiabatic cooling compensates the upward diffusion of heat in a uniformly rotating fluid and vortex stretching balances the curl of the stress. The depth, $H_L \approx 400$ m for a zonal wavelength of 1000 km, depends on the vertical stratification, the Prandtl number, and the horizontal scale.
- A Stommel–Veronis balance in which adiabatic cooling compensates the vertical diffusion of heat and vortex stretching leads to planetary vorticity advection. This balance is associated with a westward shift with height and has a vertical scale $H_{SV} \approx 700$ m for a zonal wavelength of 1000 km.
- A Sverdrup balance in which the curl of the frictional force leads to planetary vorticity advection. The depth scale is $H_S \approx 1200$ m for a zonal wavelength of 1000 km.

The results for an f-plane solution show that the fields of temperature and vertical velocity are antisymmetric about the coast. Cold air and descending motion are found to the west and warm air and ascending motion to the east. The depth of the onshore flow is well defined by the depth of the Ekman layer. Equatorward flow is produced by Coriolis deflection and decays with height consistent with the thermal wind relation. The flow is governed by the combination of the Ekman and Lineykin balances. However, the solution fails to satisfy all the lower boundary conditions [(2.16)–(2.19)].

A second solution is presented for a semigeostrophic β plane. The results indicate that the beta effect introduces a westward tilt to all the fields. The vertical velocity, which in this solution depends on the convergence/divergence of both the zonal and meridional winds, exhibits descending motion near the coast. The magnitude, however, is much smaller than that for the f-plane solution. This behavior may arise due to the offshore zonal wind, which generates ascending motion that opposes the subsidence produced by the divergence of the geostrophic wind. The flow is governed by a combination of the Lineykin, Stommel–Veronis, and Sverdrup balances. Physically the solution represents stationary diffusive Rossby waves. It fails to describe the shallower Ekman layer dynamics.

A third solution is obtained for the complete viscous problem on a β plane. The results indicate that the fields present characteristics of both the f- and β-plane solutions. All fields are tilted westward but the tilt is smaller than the one obtained for the semigeostrophic case. The meridional wind presents an equatorward flow confined to the lowest kilometer with a flow reversal aloft. The zonal flow is a maximum below 1.0 km and is onshore. There is a surface-based inversion and subsidence that extends inland. These features are only quantitatively altered by changes in the model parameters and by the inclusion of meridional thermal advection.

Application of the general solution to the region of the South American coastal desert yields good agreement with the wind profile for Lima, Peru. The agreement requires a relatively small mechanical diffusivity but a larger thermal diffusivity, consistent with a convectively unstable boundary layer. The solution displays two features characteristic of a desert environment: enhanced stability and subsidence over the coast. We may conclude that the local dynamics of the low-level flow plays a nontrivial role in the maintenance of the coastal desert.

One deficiency of the present model is the assumption of constant eddy diffusivities. Stronger daytime heating over land compared to that over the ocean will produce a large diurnal and cross-coast variation to the turbulence. The present model formulation cannot handle such temporal and spatial variations.

The model results reported here support and extend the hypothesis of Lettau (1978) and Enfield (1981) that the coastal flow is thermally forced. The current β-plane model, however, is a significant improvement over their f-plane model, which requires a prescribed vertical scale of the thermal anomaly. The shortcomings of an f-plane model without this prescription are documented in section 3a.

An apparent difficulty of a thermally forced model arises from the observation (Enfield 1981) that the longshore flow is actually stronger during an El Niño when the ocean waters are warmer. Enfield hypothesizes that this anomalous behavior arises from a decrease in coastal cloudiness leading to increased insolation over the desert and consequently a greater coastal temperature gradient. Here we note that our sensitivity studies (see Figs. 9 and 10) indicate a deeper, stronger flow for an increase in the diffusivity and a reduction in the Prandtl number without a change in the coastal thermal gradient. This behavior is consistent with Enfield's scenario that, during an El Niño, there are enhanced surface fluxes, a higher inversion (as observed), and greater mixing. We, therefore, suggest that at least a part of the observed flow intensification may be attributable to enhanced diffusivity in a more convective boundary layer.

It is important to emphasize that the model fields presented here represent a steady thermal and mechanical equilibrium that is compatible with the simple model physics and with the prescribed surface temperature anomaly. It does not ascribe a cause to the thermal anomaly. Oceanographic theories (e.g., Gill 1982) suggest that the coastal upwelling is generated by the local alongshore wind and by remote forcing from the central Pacific via an equatorial ducting of oceanic Kelvin waves. Leaving aside the issue of the remote forcing, we believe that the ultimate origin of the alongshore wind is intimately connected to the presence of the steep Andes Mountains residing along the whole length of the west coast of the continent. The role of the Andes is to block the low-level flow; the midlatitude westerlies are deflected equatorward along the west slope of the mountains (and hence the west coast of the continent) to feed the easterly trade winds. The extraordinary length of the coastal desert may be attributed to the large meridional extent of the Andes. The role of the Andes enters the present model only indirectly through the assumptions (2.12) that the meridional scale is much larger than the zonal one. Future research should seek to incorporate the Andes explicitly.

We further note that the present results are relevant not only to the South American coastal desert but also to the coastal deserts of western North America and western North and South Africa. They are all associated with coastal mountain ranges and they all possess similar climatological features: shallow equatorward flow, coastal upwelling, and a strong low-level inversion. Results of this linear model for an east coast are readily obtained by simply reversing the thermal gradient, which changes the sign of the predicted fields. For that situation we predict reduced stability, rising motion, and poleward flow along the coast. Such conditions would be more conducive for the formation of a moist rather than a dry climate. This finding is consistent with the observation that coastal deserts typically reside on the west coast of the continents, the desert of Somalia being the exception to this rule. We note the caveat that rigorous application of our results demands the satisfaction of the model assumptions (2.12). Thus, these implications for other locales are merely suggestive and not conclusive.

Finally, the model introduced here successfully incorporates the effects of friction in a β-plane boundary-layer problem. Results of the application to the South American coastal region indicate that the model with a small Prandtl number can describe well the main features of the climatology of the desert. The model is not without its shortcomings, however. Chief among them are the assumptions of a constant eddy diffusivity for the boundary-layer transports and of a uniform static stability that neglects the presence of the strong, low-level inversion. Indeed, the realistic simulation of such an inversion ultimately requires the use of a nonlinear model.

Acknowledgments. Financial support was provided in part by the National Science Foundation (NSF) under Grants ATM-8917720 and -9017043. Computer facilities were provided by the National Center for Atmospheric Research, which is sponsored by NSF. MLA thanks the Instituto Nacional de Pesquisas Espaciais in Brazil for permission and financial support to participate in the doctoral program at the Department of Meteorology of The Pennsylvania State University. She also thanks the Conselho Nacional de Desenvolvimento Científico e Tecnológico of Brazil for providing her with a scholarship.

APPENDIX

Inclusion of Meridional Cold Air Advection

We now extend the model physics to include a meridional thermal gradient, consistent with the observed sea surface temperatures of the eastern South Pacific. This gradient, assumed to be spatially uniform, alters the thermal structure of the basic state. Then the heat equation (2.6) is modified to

$$M^2 v + N^2 w = \kappa \frac{\partial^2 b}{\partial z^2}, \qquad \text{(A.1)}$$

where $M^2 = 10^{-7}\ \mathrm{s}^{-2}$ is the meridional buoyancy gra-

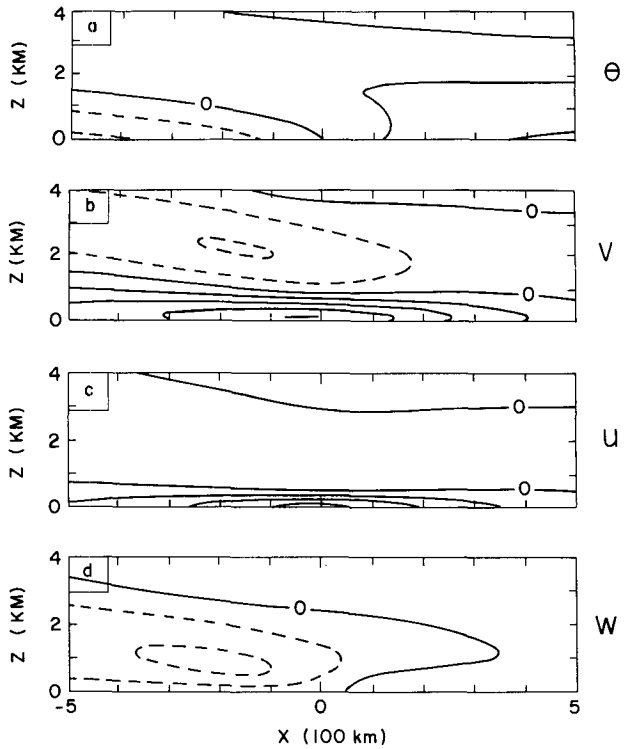

FIG. 14. As in Fig. 13 but including meridional thermal advection. Negative contours are dashed.

dient associated with a thermal gradient of about 3 K/1000 km. In writing (A.1) and retaining (2.2)–(2.5), we have ignored any mean flow of the basic state associated with M^2. Such a basic-state solution would constitute a zonally symmetric model of the trades and is beyond the scope of this investigation. Instead, we proceed in an ad hoc manner and use (A.1) to study the role of meridional thermal advection on the coastal flow.

The equations (2.2)–(2.5) and (A.1) can be combined to yield a buoyancy equation of the form

$$\frac{\eta\hat{\eta}}{f^2}\frac{\partial^8 b}{\partial z^8}+\frac{\partial^4 b}{\partial z^4}+\frac{\eta N^2}{\kappa f^2}\frac{\partial^2}{\partial x^2}\left(\frac{\partial^2 b}{\partial z^2}\right)-\frac{M^2}{f\kappa}\frac{\partial}{\partial x}\left(\frac{\partial b}{\partial z}\right)-\frac{\beta N^2}{\kappa f^2}\frac{\partial b}{\partial x}=0. \quad \text{(A.2)}$$

Meridional advection has added the fourth term on the left-hand side and does not alter the order of the governing equation. The roots associated with (A.2) are qualitatively similar to those displayed in Fig. 7 and are not shown. This similarity suggests that there is no new intrinsic balance associated with the inclusion of meridional thermal advection.

Figure 14 illustrates the effect of meridional thermal advection on the Lima case of Fig. 13. The inclusion of this thermal advection leads to a decrease in the coastal subsidence and the surface alongshore flow but an increase in the poleward flow aloft. These findings suggest that the divergence associated with the beta effect [see (3.17)] is reduced by the thermal advection and that the effect of the warm advection by the poleward flow aloft tends to offset that due to the low-level cold advection.

REFERENCES

Abreu, M. L., 1991: On the dynamics of the low-level subtropical flow along the west coast of South America. Ph.D. dissertation, Department of Meteorology, The Pennsylvania State University, 155 pp. [Available from Pennsylvania State University, University Park, PA 16802.]

Arfken, G., 1966: *Mathematical Methods for Physicists, second ed.* Academic Press, 815 pp.

Chu, P. C., 1985: A boundary layer theory of coastal desert formation and sea breeze circulation. Ph.D. dissertation, Department of Geographical Sciences, The University of Chicago, 194 pp. [Available from University of Chicago, Chicago, IL 60637.]

Enfield, D. B., 1981: Thermally driven wind variability in the planetary boundary layer above Lima, Peru. *J. Geophys. Res.*, **86,** 2005–2016.

Gill, A. E., 1982: *Atmosphere-Ocean Dynamics*. Academic Press, 662 pp.

Lanczos, C., 1956: *Applied Analysis.* Prentice-Hall, 539 pp.

Leetmaa, A., 1971: Some effects of stratification on rotating fluids. *J. Atmos. Sci.*, **38,** 65–71.

Lettau, H. H., 1978: Introduction. *Exploring the World's Driest Climate,* H. H. Lettau and K. Lettau, Eds., University of Wisconsin Press, 12–29.

Lineykin, P. S., 1955: On the determination of the thickness of the baroclinic layer in the ocean. *Dokl. Akad. Nauk. SSSR,* **101,** 461–464.

Lydolph, P. E., 1973: On the causes of aridity along a selected group of coasts. *Coastal Deserts—Their Natural and Human Environments,* D. H. K. Amiran, and A. W. Wilson, Eds. The University of Arizona Press, 67–72.

Mahrt, L. J., 1980: Boundary layer mean flow dynamics. *Workshop on the Planetary Boundary Layer,* J. C. Wyngaard, Ed. Boston, Amer. Meteor. Soc., 322 pp.

——, and W. Schwerdtfeger, 1970: Ekman spirals for exponential thermal wind. *Bound.-Layer Meteor.,* **1,** 137–145.

Oort, A. H., 1983: Global Atmospheric Circulation Statistics 1958–1973. NOAA Prof. Paper 14. [Available from Superintendent of Documents, U.S. Govt. Printing Office, Washington, D.C. 20402.]

Panofsky, H. A., and J. A. Dutton, 1984: *Atmospheric Turbulence.* Wiley, 397 pp.

Prohaska, F. J., 1973: New evidence on the climatic controls along the Peruvian coast. *Coastal Deserts—Their Natural and Human Environments,* D. H. K. Amiran, and A. W. Wilson, Eds., The University of Arizona Press, 91–107.

Riehl, H., 1979: *Climate and Weather in the Tropics.* Academic Press, 611 pp.

Schemenauer, R. S., H. Fuenzalida, and P. Cereceda, 1988: A neglected water resource: The Comanchaca of South America. *Bull. Amer. Meteor. Soc.,* **69,** 138–147.

Smagorinsky, J., 1953: The dynamical influence of large-scale heat sources and sinks on the quasi-stationary mean motions of the atmosphere. *Quart. J. Roy. Meteor. Soc.,* **79,** 342–366.

Stommel, H., and G. Veronis, 1957: Steady convective motion in a horizontal layer of fluid heated uniformly from above and cooled non-uniformly from below. *Tellus,* **9,** 401–407.

Taylor, G. I., 1915: Eddy motion in the atmosphere. *Phil. Trans. Roy. Soc. London,* **A215,** 1–26.

Trewartha, G. T., 1981: *The Earth's Problem Climates.* University of Wisconsin Press, 371 pp.